ISIJ International, Vol. 52 (2012), No. 8, pp. 1394–1403

Kinetic Analysis of the Decomposition Reaction of CH_4 Injecting into Molten Slag

Yoshiaki KASHIWAYA[1)]* and Masami WATANABE[2)]

1) Formerly Graduate School of Hokkaido University. Now at Graduate School of Energy Science, Kyoto University, Yoshida Honmachi, Sakyoku, Kyoto, 606-8501 Japan. 2) Hokkaido Sumiden Precision Co., Ltd., Naie-cho, Hokkaido, 079-0304 Japan.

(*Received on January 17, 2012; accepted on May 17, 2012*)

Utilization of heat of slag is key technology for the reduction of CO_2 emission in steel industries. While hydrogen production is important for the society of aiming to the sustainable energy system, the green hydrogen must be produced for the actual CO_2 reduction.

In the present study, methane gas was injected into a molten slag and hydrogen was produced through the thermal decomposition reaction.

$CH_4 = C + 2H_2$

Kinetic analysis was performed using an graphite crucible both with empty and slag. The rate constants for the graphite crucible, k_G and the slag, k_S, were obtained separately.

The rate constants for graphite surface and slag surface, k_G and k_S, respectively, are as follows:

$$k_G / cm \cdot s^{-1} = 41.74 \times \exp\left(-\frac{51\,741}{RT}\right) \pm 0.05$$

$$k_S / cm \cdot s^{-1} = 4.053 \times 10^6 \times \exp\left(-\frac{190\,310}{RT}\right) \pm 0.05$$

Using the obtained rate constants, the increase of the area of reaction surface during the CH_4 injection was estimated.

It was found that the slow soaking of the injecting lance could be utilized for the heat of molten slag. In addition, the slag shape can be a powder type through the injection of CH_4.

KEY WORDS: decomposition of CH_4; kinetic analysis; rate constant; molten slag; injecting of methane.

1. Introduction

Hydrogen is the secondary energy and some extent of CO_2 will be produced in a process of its production, more or less. A green hydrogen means that no CO_2 is exhausted on the way of production, and a black hydrogen means that same moles of CO_2 are exhausted. Between green and black, there is a gray hydrogen which is some extent of CO_2 exhausted.

Generally, most of hydrogen belongs to gray hydrogen and we should approach to the production of green hydrogen for actual CO_2 reduction.

The source of hydrogen would be the natural gas, biomass and water, while the energy of hydrogen production could be the atomic energy, natural energies and the waste heats in the industries. There are many kinds of waste heats existing in the steel industries and its utilization were investigated by many researchers in the research group "Science and Technologies for the Effective Use of Unrecovered Energy in Steelworks" of ISIJ (Iron and Steel Institute of Japan).[1–17)]

In the Research Group, the authors have studied on the heat recovery from slag using Rotary Cylinder Atomizing Method (RCAM).[4–6)] It is good method to get a fine spherical slag beads more than 200 μm. However, some of heat was lost during the atomizing process and it is difficult to find the way of utilization of spherical slag beads. It is necessary to develop the demand for spherical slag.

On the other hand, a gas injecting method can obtain the good contact between the gas and molten slag, which means that the efficiency of heat recovery from slag can be maximum, although it is depending on the size of bubble and its distribution. Furthermore, when methane gas could be used as a injecting gas, the reaction (1) occurs and hydrogen can be obtained. The meaning of this method is that the sensible heat of slag can be changed into a chemical energy by using an endothermic reaction.

$$\mathbf{CH_4\ (g) \rightarrow C + 2H_2\ (g)}\ \Delta H^o_{298}/\mathrm{kJmol^{-1}} = \mathbf{74.6} \quad \ldots(1)^{18)}$$

$$\Delta G^o/\mathrm{kJmol^{-1}} = 88.039 - 0.1079\ T\ (573\ \mathrm{K} - 1\,773\ \mathrm{K}) \quad \ldots..(2)^{18)}$$

Thermodynamically, the reaction (1) can occur from 816 K,

* Corresponding author: E-mail: kashiwaya@energy.kyoto-u.ac.jp
DOI: http://dx.doi.org/10.2355/isijinternational.52.1394

but kinetically, the reaction become dominant from 1 073 K without any catalyst. The decomposition reaction (1) is an endothermic one and the enthalpy change at 298 K is ΔH^{o}_{298}/kJmol^{-1}=74.6. If a sensible heat of BF (blast furnace) slag in one ton from 1 773 K to 1 073 K could be used for the reaction (1), total heat was 275 Mcal,[19] by which 8.5 kmol (190 Nm^3) of CH_4 gas could be decomposed and 17 kmol (380 Nm^3) of H_2 gas could be produced (the calculation was performed with the assumption: CH_4 gas of 8.5 kmol at 298 K $\rightarrow$ H_2 gas of 17 kmol and carbon of 8.5 kmol at 1 073 K). The amount of H_2 corresponds to the one in COG (coke oven gas) evolved in the course of about 500 kg-coke production.

In this study, kinetics of CH_4 decomposition during the injection into the slag melt was studied. To clarify the phenomena during injection, the reaction rates were measured through two separate experiments, the one was carried out by the graphite crucible (without slag) and the other was carried out by the graphite crucible having slag melt. From the kinetic analysis, the rate constants for the graphite surface and the slag surface were separated. Using the obtained rate constants, the decomposition reaction during injection into the slag melt was evaluated. It was found that the method of injection affected strongly on the area of reaction surface.

2. Experimental

2.1. Apparatus and Procedure

Figure 1 shows a schematics of experimental apparatus. Methane (CH_4) gas used is a high purity of 99.9% and an argon gas is an ultra high purity of 99.9999%. The flow rates of both gases were adjusted to a desired one by MFC (Mass Flow Controller), precisely. The total flow rate of Ar+CH_4 mixture was 1 000 cm^3/min (STP), and the flow rate of CH_4 was changed to two levels, 500 cm^3/min (STP) and 700 cm^3/min (STP) as shown in **Table 1**.

The reaction gas mixture was introduced into the reaction tube through the alumina lance (4 mmϕ I.D. $\times$ 6 mmϕ O.D, 600 mmL).

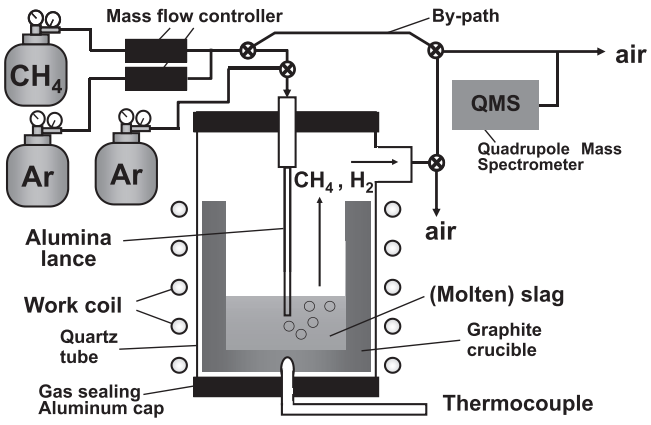

Fig. 1. Schematics of experimental apparatus.

Table 1. Gas flow rate of reaction gas (CH_4–Ar mixture (Ncm^3/min)).

	Total Flow rate Ar+CH_4 (Ncc/min)	CH_4 Flow rate (Ncc/min)	Range of temperature
Condition-1	1 000	500	1 000°C–1 550°C
Condition-2	1 000	700	1 000°C–1 550°C

The slag sample was melted in a graphite crucible (33 mmϕ I.D. $\times$ 46 mmϕ O.D. $\times$ 90 mm Depth and 110 mm in height). The weight of slag was 74 g. When the slag was melted in the graphite crucible, the depth of slag melt was 3 cm.

The graphite crucible having slag sample was heated by an induction furnace with 15 kW and 40 kHz. The sample and graphite crucible were set in the quartz reaction tube which was sealed with water cooled aluminum gas tight caps in both ends. Temperature of the sample was measured by B-type (Pt-6Rh, Pt-30Rh) thermocouple which was located at the bottom of graphite crucible.

All experiments were heating up to a given temperature (Table 1) under Ar atmosphere, when the alumina lance was located 5 mm from slag surface. On the other hand, the reaction gas (Ar+CH_4 mixture) was adjusted to a desired composition in a by-pass (Fig. 1) and a calibration of QMS (quadrupole mass spectrometer) was performed, simultaneously. The details of QMS calibration was mentioned below.

When the calibration was done, and the temperature and the flow rate became stable, the argon gas for purge was stopped and the reaction gas mixture was introduced to reaction tube. Almost at the same time, the gas blowing lance was immersed into slag melt. The position of end of lance was located about 5 mm from the bottom of crucible.

The downward velocity of lance affects the result of injection significantly. There are two downward velocities selected in this experiment. One is 0.6 cm/s which means a quick soaking of lance and actually the lance is moved from the surface of slag to bottom of crucible about 3 cm within 5 s, the other is slow soaking and about 0.03 cm/s, which means that the lance was moved stepwise for 0.5 cm in every 15 s.

2.2. Gas Analysis Using QMS (Quadrupole Mass Spectrometer)

QMS (ThermoStar produced by Pfeiffer Vacuum GmbH) was used for the quantification analysis of gases. Recently, a software for the gas quantification is prepared in the respective system, however in this experiment, the quantification method was adopted as shown in below.[20]

Quantification analysis using QMS is relatively difficult, because the condition around the quadrupole in a analysis tube, where is under high vacuum, is varied by the gas composition and the amount of gas introduced. The adsorbed gases inside the analysis tube affects the total pressure, which has large effect on the intensities. Furthermore, the amount of the adsorbed gases is also varied with the kind of gases. Since the QMS has quite high sensitivity until the order of ppb, the establishment of the quantification method can be helpful for a gas related experiment. The usage of inert dilute gas (argon), which is always constant flow rate, can cancel these disadvantages of QMS. Although the intensities are varied with the total pressure, the objective intensities can be available through the normalization by the argon intensity. Fundamental equation is expressed by Eq. (3),

$$I_i/I_{Ar} = a_i + \sum_j^n b_j V_j / V_{Ar} \quad \text{..... (3)}$$

where, I and V mean the intensity of QMS and flow rate (cm^3/min (STP)), respectively. The subscript means the gases related. $\boldsymbol{a}$ and $\boldsymbol{b}$ are coefficients for determining the calibration curve. According to the kinds of gas, the existence of fragment peak must be taken into account to the calibration curve.

For example, in the case of Ar–CO–CO_2 system, CO_2 makes a fragment of CO gas, which will disturb the analysis of CO gas. Equation (3) can formulate as Eq. (4).

$$\boldsymbol{I_{CO_2}/I_{Ar} = a_{CO_2} + b_{CO_2}V_{CO_2}/V_{Ar} + b_{CO}V_{CO}/V_{Ar}} \quad \text{..... (4)}$$

In this experiment, H_2 could be a fragment peak of CH_4. However, the fragment peak from CH_4 can minimize, when an adequate analyzing condition such as a ionization voltage and emission current are selected. The examples of fragment peaks by QMS are shown in **Fig. 2** in comparison with the different gas flowing path. In Fig. 2(a), result of QMS is shown, when the gas mixture (Ar+CH_4) was flowed to the 'by-path'. On the other hand, in Figs. 2(b) and 2(c), the gas mixture was introduced into the reaction tube in which the slag was already melted at 1 500°C. The decomposition reaction of CH_4 expressed by Eq. (1) must occur and hydrogen evolved. In Fig. 2(a), there is no H_2 peak observed, because the conditions (Emission current: 1.0 mA, Applied Voltage for MCP (Multi Channel Plate): 600 V) of QMS analysis were adequately selected. The other fragments, CH^+, CH_2^+, CH_3^+ come from CH_4 and Ar++ come from Ar. Those fragments form in ion-chamber of QMS device by a collision with electrons, however, the existence of those fragments does not disturb the quantification analysis of CH_4 and H_2. When the gas mixture is introduced to the reaction tube, the decomposition reaction was promoted and H_2^+ corresponding to H_2 generation was detected. The other peaks ($C_2H_2^+$, $C_2H_4^+$) related to C_2 compounds were negligible as shown in Figs. 2(b) and 2(c).

The decomposition mechanism of CH_4 between the inside of QMS and the reaction tube resembles each other. There are enormous researches related to the CH_4 decomposition and the reaction mechanisms are summarized on NIST data base.[21] The decomposition sequence is generally expressed as follows:

$$\begin{aligned} &CH_4(g) \rightarrow CH_3{*}(\text{radical}) \rightarrow CH_2{*}(\text{radical}) \\ &\rightarrow CH{*}(\text{radical}) \rightarrow C\ (\text{soot}) \quad \text{..... (5)} \end{aligned}$$

The details of reaction in the graphite crucible and slag system are discussed in the later section.

Finally, the equation of calibration can be simplified as shown in Eqs. (6) and (7).

$$\boldsymbol{I_{CH_4}/I_{Ar} = a_{CH_4} + b_{CH_4}V_{CH_4}/V_{Ar}} \quad \text{..... (6)}$$

$$\boldsymbol{I_{H_2}/I_{Ar} = a_{H_2} + b_{H_2}V_{H_2}/V_{Ar}} \quad \text{..... (7)}$$

The obtained calibration lines for H_2 and CH_4 are shown in **Fig. 3**. The error of analysis was ±0.5% for H_2 and ±1.0% for CH_4. These calibration lines were measure in every experiments, because the condition of analysis tube of QMS would change gradually with time.

2.3. Slag Sample

Slag sample is BF (blast furnace) slag which is water quenched (water granular) slag.

The chemical composition of the slag is shown in **Table 2**. The basicity (C/S=CaO/SiO_2) is 1.28 and the content of MgO is 6.28 mass%. As mentioned above, the weight of slag is 74 g and the volume of melt is 25.65 cm^3. The density of slag melt is 2.88 g/cm^3.

2.4. Kind of Experiment

In this study, experiments are classified into three groups.

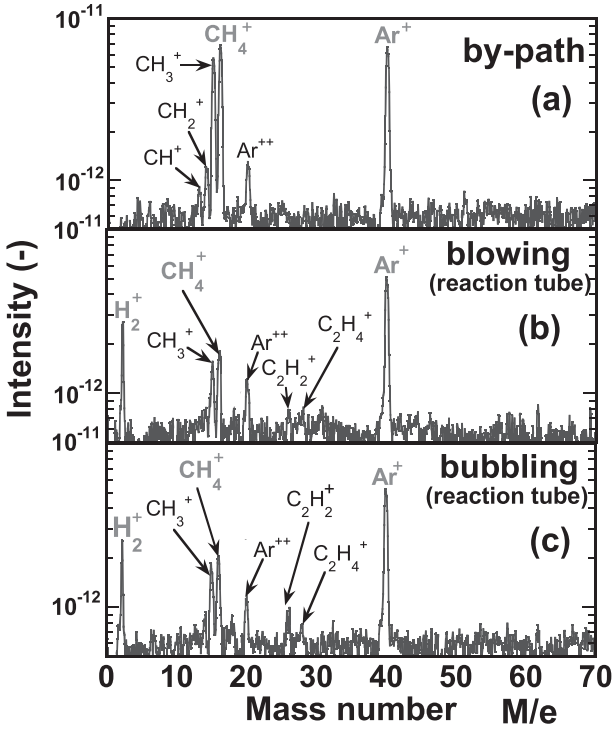

Fig. 2. Fragment peaks during QMS analysis of Ar–CH_4 mixture.

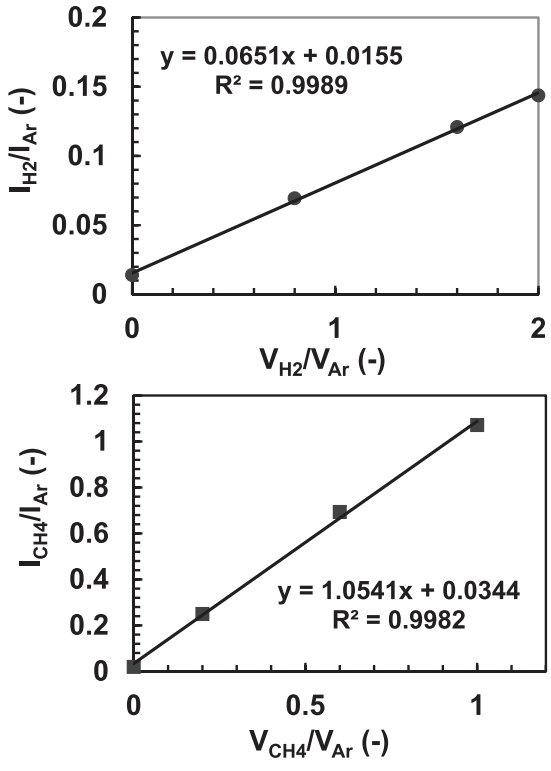

Fig. 3. Calibration lines of H_2 and CH_4 by QMS.

Table 2. Chemical composition of BF slag (mass%).

	CaO	SiO_2	Al_2O_3	MgO	FeO	Mn	P_2O_5	C/S
BF slag	42.99	33.52	13.77	6.28	0.37	0.27	<0.02	1.28

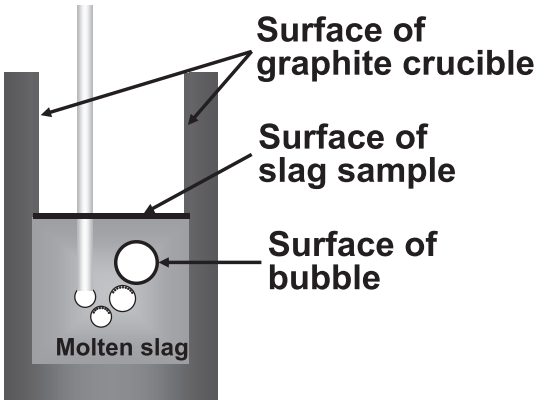

Fig. 4. Reaction surfaces during bubbling of CH_4.

(i) EXP-1: Injection into slag melt
(ii) EXP-2: Blowing into the empty graphite crucible
(iii) EXP-3: Blowing into the graphite crucible with slag

Main experiment is the injection experiment, hereinafter, it is called as EXP-1 for convenience. The lance for injection is a single hole alumina tube and the inner diameter is 4 mmϕ. The size and number of hole in lance is important, because the size of bubble, which is related to the total surface area of reaction, can be decided by the property of hole.

In this study, the number of hole in lance was fixed to a single one. The lance was waiting at 5 mm over slag surface before injection, then, the lance was moved downward into the slag. Since the downward velocity is also important factor to affect the injection behavior, it was changed in two levels. Two kind of injection experiment are carried out as follows:

(i-1) EXP-1-1: lance downward velocity is 8.3 mm/s (moving 25 mm in 3 s).
(i-2) EXP-1-2: lance downward velocity is 0.33 mm/s (moving 25 mm in 75 s).

The reaction is a large endothermic one which would solidify the slag rapidly, so that the lance velocity affect the rising behavior of gas bubbles accompanied with the solidification of slag.

Moreover, the reaction will also occur in the inner surface of graphite crucible, slag surface and inner surface of bubble as shown in **Fig. 4**. It is necessary to distinguish the reaction rate among three different surfaces. However, in this study, it was assumed that the reaction rate between slag surface and inner surface of bubble in slag was almost the same. Then, the fundamental experiments to distinguish the reaction rates between graphite surface and slag surface have been performed using two different crucibles as shown in **Fig. 5**. Figure 5(a) shows a graphite crucible without slag by which the reaction rate on the graphite surface can be measured (EXP-2). The area of reaction surface of graphite crucible is A_G (101.86 cm^2). The end position of alumina lance is 5 mm from the bottom of graphite crucible. Figure 5(b) shows a graphite crucible with slag, by which the reaction

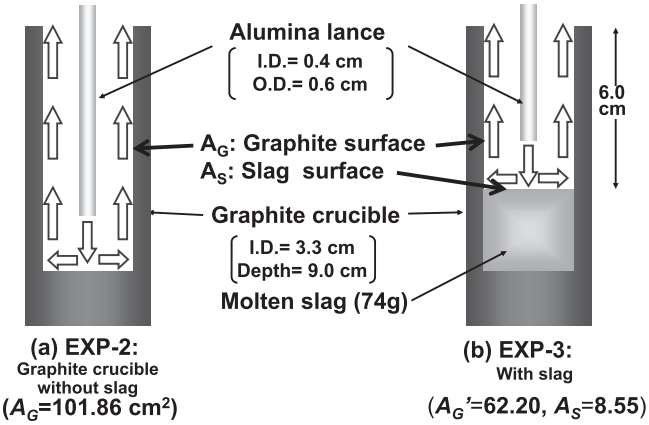

Fig. 5. Fundamental experiment of CH_4 decomposition without bubbling.

rates for the graphite surface and the one for slag surface are obtained (EXP-3). The area of graphite surface is 62.2 cm^2 and the slag surface is 8.55 cm^2. The end position of alumina lance is 5 mm from the surface of slag melt.

From the result of EXP-3, a mixed reaction rates between the graphite surface and slag surface will be obtained. Then, using the result of EXP-2, the single rate of slag surface can be estimated.

3. Results and Discussion

3.1. Fundamental Experiment

Figures 6(a) and 6(b) show the typical results of EXP-2 and EXP-3, respectively. When the reaction gas was introduced to the reaction tube, CH_4 quickly decreased and H_2 gas increased. As there was relatively large dead space, some evolved H_2 gas stagnated in the dead space. From this reason, it took a long time to substitute completely as shown by the region indicated by hatching.

According to the endothermic reaction of CH_4 decomposition, temperature started to decrease and showed a given constant value, when the reaction became steady state. **Figure 7** shows the temperature decrease from initial temperature to the end of experiment (Final Tempe.). From Fig. 7, the decrease of temperature become large in high temperature in accordance with the increase of reaction rate. For example, the temperature decrease was about 90 K at 1 600 K and almost negligible at 1 073 K. In the case of the kinetic analysis, the final temperature, at which the reaction reached to the steady state, was used.

At the end of experiment, the reaction gas was changed to the by-path and the reaction was stopped. As shown in Fig. 6, the CH_4 gas was quickly returned to the initial flow rate and H_2 gas went to zero.

The decomposed CH_4, $V^d_{CH_4}$ (Ncm^3/min) was calculated by Eq. (8).

$$V^d_{CH_4} = V^i_{CH_4} - V^o_{CH_4} \quad \text{..... (8)}$$

where $V^i_{CH_4}$ and $V^o_{CH_4}$ are inlet and outlet flow rate (Ncm^3/min) of CH_4, respectively.

The decomposed CH_4 flow rate obtained, $V^d_{CH_4}$ were plotted in **Fig. 8**. Results of EXP-2 (graphite crucible without slag) are shown by ●, ○ and ▲, while results of EXP-3 are shown by ⊘, ⊗ and ■. The marks of ●, ○, ⊘ and ⊗

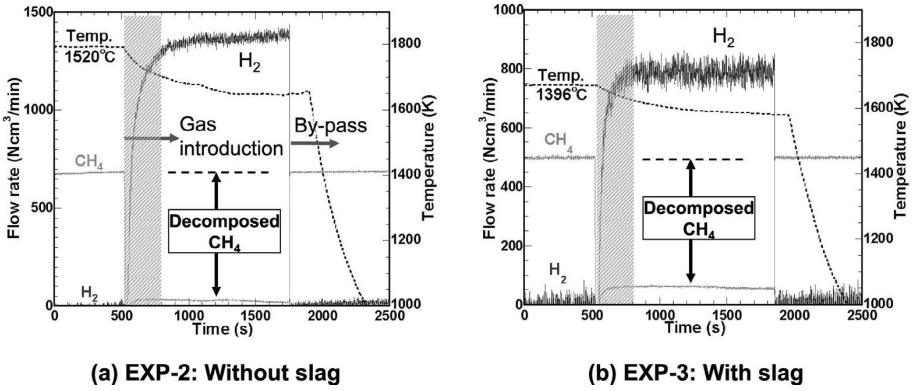

(a) EXP-2: Without slag **(b) EXP-3: With slag**

Fig. 6. Typical experimental results for the fundamental experiments (a) without slag, 1 793 K, 700 Ncm^3/min, (b) with slag, 1 669 K, 500 Ncm^3/min.

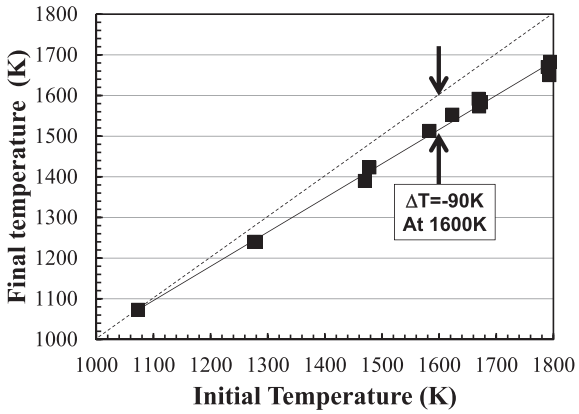

Fig. 7. Temperature change between initial and final of experiment.

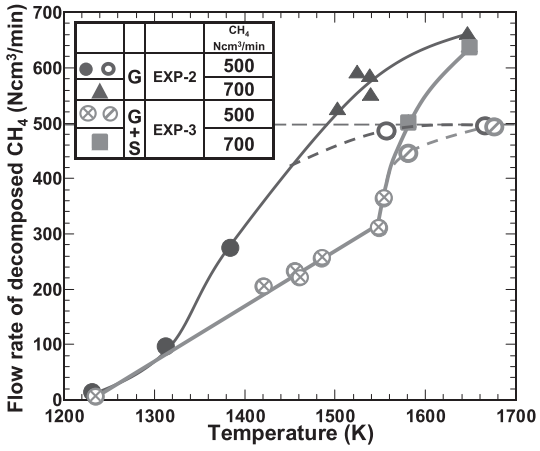

Fig. 8. Flow rates of Decomposed CH_4 in EXP-2 and EXP-3.

correspond to the flow rate of 500 Ncm^3/min. ▲ and ■ correspond to 700 Ncm^3/min. In the higher temperature range more than 1 540 K and 500 Ncm^3/min (○ and ⊘), the reaction gas CH_4 was completely consumed and the reaction did not in the steady state, which was expressed by the broken line in Fig. 8. Then the experiments with higher flow rate of 700 Ncm^3/min were performed and the results were plotter with ▲ and ■.

Decomposition reaction gradually became dominant from about 1 240 K both in EXP-2 and EXP-3. However, the apparent decomposition rate $V^d_{CH_4}$ in EXP-2 (graphite crucible) was higher than that of EXP-3 (graphite crucible with slag) in the temperature range higher than 1 300 K. The result was simply caused by the difference of reaction surface area. As shown in Fig. 5, the area of reaction surface in EXP-2 (graphite crucible), A_G is 101.86 cm^2, while the area in EXP-3 (graphite crucible with slag) is 70.75 cm^2 (A'_G=62.20 cm^2, A_S=8.55 cm^2). The simple calculation of the apparent reaction rate for EXP-2 is about 1.5 times higher than that of EXP-3.

In the case of EXP-3, the apparent decomposition rate $V^d_{CH_4}$ increased from about 1 540 K, from which the slag would start to melt. All these temperatures are adopted at end of experiment as mentioned above (Fig. 7), because the kinetic analyses were performed with the temperature under the steady state. Initial temperatures must be higher than the ones shown in Fig. 8. When the temperature of EXP-3 was 1 540 K at the end of experiment, the initial temperature was 1 640 K which was closed to the melting point of the slag used.[22] This result means that the CH_4 decomposition enhanced by the existence of slag melt. The details must be discussed after the kinetic analysis below.

3.2. Kinetic Analysis

Using the results of EXP-2 and EXP-3, kinetic analysis was performed and the rate constants for the graphite surface, k_G and for the slag surface, k_S were determined.

Assuming the first order reaction, the rate equation of decomposition reaction can be expressed by Eq. (9).

$$r = Ak\left(C^i_{CH_4} - C^e_{CH_4}\right) \quad \text{..... (9)}$$

where, r is the reaction rate (mol/s), k is the rate constant (cm/s) and A is the reaction surface area. $C^i_{CH_4}$ and $C^e_{CH_4}$ are the concentration of methane in the initial reaction gas (mol/cm^3) and the concentration at equilibrium obtained by Eq. (1), respectively. The concentrations of methane are determined by Eqs. (10) and (11),

$$C^i_{CH_4} = \frac{P^i_{CH_4}}{R \cdot T} \quad \text{..... (10)}$$

$$C^e_{CH_4} = \frac{P^e_{CH_4}}{R \cdot T} \quad \text{.....(11)}$$

where $P^i_{CH_4}$ can be obtained using the experimental flow rate $V^i_{CH_4}$, V^i_{Ar} by Eqs. (12) and (13).

$$V^i_{CH_4} + V^i_{Ar} = V_T \quad \text{..... (12)}$$

$$V^i_{CH_4} / V_T = P^i_{CH_4} \quad \text{..... (13)}$$

$P^e_{CH_4}$ can be obtained based on Eqs. (14) and (15) as follows:

$$\Delta G^0 = -RT \ln\left(\frac{\left(P^e_{H_2}\right)^2}{P^e_{CH_4}}\right) \quad \text{..... (14)}$$

$$\Delta G^0 = 88.039 - 0.10789\ T\ [\text{kJ/mol}] \quad \text{..... (15)}$$

where $P^e_{CH_4}$ and $P^e_{H_2}$ are equilibrium partial pressure of methane and hydrogen, respectively. The temperature dependence of ΔG^0 was obtained using thermochemical data base.[18] Since the total hydrogen content is not change before and after the reaction, Eq. (16) can be established.

$$2V^i_{CH_4} = 2V^e_{CH_4} + V^e_{H_2} \quad \text{.....(16a)}$$

$$P^e_{CH_4} = \frac{V^e_{CH_4}}{V^e_T}, \quad P^e_{H_2} = \frac{V^e_{H_2}}{V^e_T} \quad \text{..... (16b, c)}$$

where

$$V^e_T = V^i_{Ar} + V^e_{CH_4} + V^e_{H_2} \quad \text{..... (16d)}$$

Then, $V^e_{CH_4}$ can be obtained by Eq. (17),

$$V^e_{CH_4} = \frac{(2V^i_{CH_4} + \frac{V^e_T}{4}G) \pm \sqrt{\left(2V^i_{CH_4} + \frac{V^e_T}{4}G\right)^2 - 4\left(V^i_{CH_4}\right)^2}}{2} \quad \text{..... (17)}$$

where $G=\exp(-\Delta G^0/RT)$ from Eq. (14), and the hydrogen in equilibrium can be obtained by the mass balance of hydrogen, $V^e_{H_2} = 2V^i_{CH_4} - 2V^e_{CH_4}$. $P^e_{CH_4}$ obtained by Eq. (16b) are shown in **Fig. 9** for the conditions of $P^i_{CH_4} = 0.5$ (500 cm^3/min (STP)) and $P^i_{CH_4} = 0.7$ (700 cm^3/min (STP)). In the low temperature range from 1 100 K to 1 300 K, the equilibrium partial pressures of CH_4, are relatively high and from about 0.15 to 0.02. However, it is very low in the higher temperature range and can be negligible more than 1 500 K.

In the case of graphite crucible, EXP-2, the reaction equation can be written by Eq. (18).

$$r = A_G k_G (C^i_{CH_4} - C^e_{CH_4}) \quad \text{..... (18)}$$

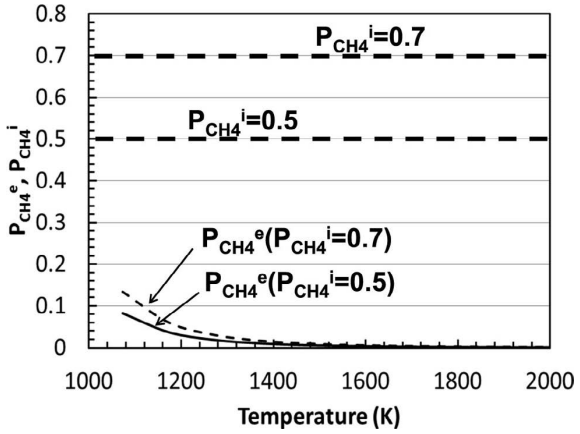

Fig. 9. Relationship between $P^e_{CH_4}$ and $P^i_{CH_4}$.

While, in the case of EXP-3 for the graphite crucible with slag, the reaction equation is Eq. (19).

$$r = A'_G k_G (C^i_{CH_4} - C^e_{CH_4}) + A_S k_S (C^i_{CH_4} - C^e_{CH_4}) \quad \text{..... (19)}$$

Equation (19) can be rewritten as follows:

$$r = k'(C^i_{CH_4} - C^e_{CH_4}) \quad \text{..... (20)}$$

where $k' = A'_G k_G + A_S k_S$. Since the k' and k_G can be obtained by EXP-3 and EXP-2, respectively, k_S can be estimated. The obtained k_G and k_S are expressed by Eqs. (21) and (22), respectively, and plotted in **Fig. 10**. The linear relationships of temperature dependence for k_G and k_S for the different gas flow rate are obtained. The activation energy of k_G is 51 kJ/mol and the one of k_S is 190 kJ/mol, which is extremely high value. Below 1 450 K (1 177°C), k_S is lower than k_G. However, in the higher temperature region, k_S become higher value than k_G, which is corresponding to the phenomena of slag softening and melting. At 1 680 K, the value of k_S is about 4.77 times larger than k_G. The mechanism of enhancement of CH_4 decomposition by molten slag was discussed below.

$$k_G / cm \cdot s^{-1} = 41.74 \times \exp\left(-\frac{51\,741}{RT}\right) \pm 0.05 \quad \text{..... (21)}$$

$$k_S / cm \cdot s^{-1} = 4.053 \times 10^6 \times \exp\left(-\frac{190\,310}{RT}\right) \pm 0.05 \quad \text{... (22)}$$

3.3. Mechanism of CH_4 Decomposition and Effect of Molten Slag

There are many reviews and papers related to the CH_4 decomposition[23–27] and the kinetic database is available on the WEB site of NIST (National Institute of Standard and Technology).[21] The elementary reactions of decomposition of CH_4 are considered as follows:

$$CH_4 \rightleftarrows CH_3^* + H^*, \qquad Ea = 264\sim430\ \text{kJ} \quad \text{..... (23)}$$

$$CH_3^* \rightleftarrows CH_2^* + H^*, \qquad Ea = 352\sim383\ \text{kJ} \quad \text{..... (24)}$$

$$CH_2^* \rightleftarrows CH^* + H^*, \qquad Ea = 348\sim375\ \text{kJ} \quad \text{..... (25)}$$

$$CH^* \rightleftarrows C^* + H^*, \qquad Ea = 280\ \text{kJ} \quad \text{..... (26)}$$

where the superscript '*' means a radical state of species.

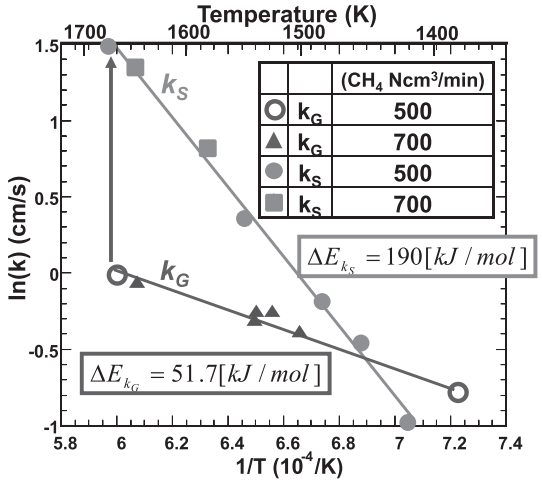

Fig. 10. Arrhenius plots of k_G and k_S.

Then, the reactions with radical hydrogen H* are as follows:

$$CH_4 + H^* \rightleftarrows CH_3^* + H_2, \quad Ea=45\sim60 \text{ kJ} \quad (27)$$

$$CH_3^* + H^* \rightleftarrows CH_2^* + H_2, \quad Ea=63 \text{ kJ} \quad (28)$$

$$CH_2^* + H^* \rightleftarrows CH^* + H_2, \quad Ea=-5.6\sim -7.48 \text{ kJ} \quad (29)$$

$$CH^* + H^* \rightleftarrows C^* + H_2, \quad Ea=0.67 \text{ kJ} \quad (30)$$

Actually, much soot precipitated in the experiment.

$$nC^* \rightleftarrows Cn \text{ (soot)} \quad (31)$$

The rate constants k are expressed by Eq. (32).

$$k(T)=A \exp(-Ea/RT) \quad (32)$$

where 'A' is a Frequency factor and 'Ea' is an activation energy.

The unit of k is cm^3 $molecule^{-1}$ s^{-1}. All values are obtained from NIST database.[21] In the present study, the activation energies, Ea (kJ/mol) were compared with the ones obtained in this experiment, because the unit of rate constant k (cm^3 $molecule^{-1}$ s^{-1}) was different from the present experiment k (cm/s).

The activation energy, 51.7 kJ for graphite crucible is excellent agreement with the one for Eq. (27). J. W. Sutherland *et al.*[28] has shown the activation energy, 57 kJ for the reaction $CH_4+H^* \rightleftarrows CH_3^* + H_2$ (Eq. (27)) and the Arrhenius type equation was expressed by Eq. (33).

$$k_1=2.935\times10^{-10}\exp(-6\,934/T) \quad cm^3 \text{ molecule}^{-1} \text{ s}^{-1} \quad (33)^{28}$$

Furthermore, the thermodynamic equilibrium constant $K_{1,2}=k_1/k_2$, where k_1 is the rate constant of forward reaction and k_2 is backward reaction for Eq. (27), was shown by Sutherland.[28]

$$K_{1,2}=39.514-2.7804\times10^4T^{-1}+7.9684\times10^6T^{-2}-8.2897\times10^8T^{-3} \quad (800 \text{ K} \leqq T \leqq 2\,000 \text{ K}) \quad (34)^{28}$$

Using the equilibrium constant $K_{1,2}$, non-linear rate constant k_1 was shown by them.

$$k_1=6.78\times10^{-21}T^{3.156}\exp(-4\,406/T), \text{ cm}^3 \text{ molecule}^{-1} \text{ s}^{-1} \quad (35)^{28}$$

The apparent activation energy of Eq. (35) for the equation type of Eq. (33) is 69 kJ, which is relatively higher than that of the present value, however, it is within the range of error.

On the other hand, the rate constant for slag, ks is very high in the high temperature range from 1 450 K to 1 700 K in which the slag is melted. The activation energy of ks is also very high and 190 kJ. However, the activation energies for Eqs. (23)–(26) are 280 kJ to 380 kJ, which are extremely higher than that in this experiment. The reaction mechanism of CH_4 decomposition in the existence of slag melt should be different from ordinary decomposition reaction (Eqs. (23)–(30)). In this study, the reaction mechanism of CH_4 decomposition in cooperation with slag melt was considered as shown in **Fig. 11**. After experiment, the surface of slag was observed (Fig. 11(b)). There was a smaller circle on the surface where the reaction gas from alumina lance was impinging. The surface in the center circle was depressed by the pressure of gas. Moreover, the periphery of the center circle showed a shape of valley, to which a reaction mechanism of gas evolution might be related. In addition, the position of meniscus between graphite crucible and slag surface has little carbon film, while most of the slag surface was covered with carbon film. If the carbon film on the slag surface provided the reaction sites for the decomposition of CH_4, the effective slag surface would be changed by the formation of carbon film. However, the obtained rate constants of k_G and k_S showed the linear nature on the reaction temperature under the assumption of constant surface areas for graphite and slag, so that the carbon film formed would not affect the decomposition reaction of CH_4 actually.

From these results, the elementary reactions of the CH_4 decomposition on the surface of molten slag are considered as follows:

$$CH_4 \text{ (g)} \rightleftarrows CH_4 \text{ (ad)} \quad (36)$$

$$CH_4 \text{ (ad)} \rightleftarrows C\text{(ad)} + 4H \text{ (ad)} \quad (37)$$

$$H \text{ (ad)} \rightleftarrows \underline{H} \text{ (in slag)} \quad (38)$$

$$\underline{2H} \text{ (in slag)} \rightleftarrows H_2 \text{ (g)} \quad (39)$$

where 'ad' means the state of adsorption on the surface of slag, and the under-line means the state of dissolution in slag. At first, the CH_4 gas adsorbed on the surface of slag

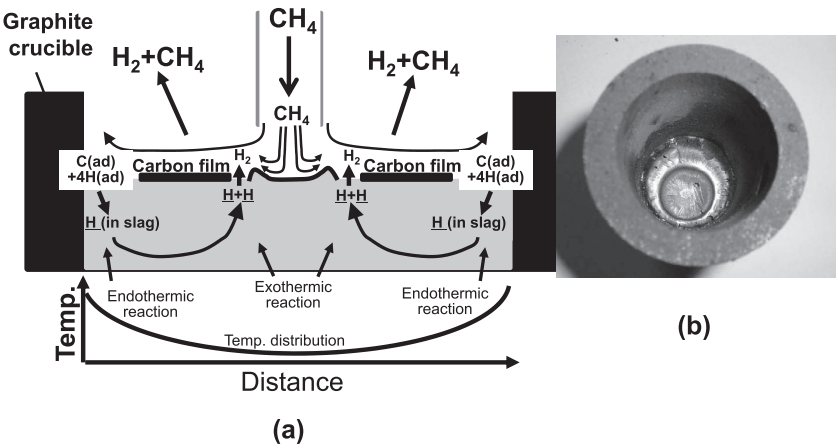

Fig. 11. (a) Reaction mechanism of CH_4 decomposition in cooperation with slag melt and (b) top view of slag surface in the graphite crucible after experiment.

melt as expressed by Eq. (36). Then, the CH_4 decomposes into C (ad) and H (ad) (Eq. (37)), simultaneously, the H (ad) dissolve into slag melt (Eq. (38)) as a $\underline{H}$ (in slag) which is a kind of radical species. Equation (37) is an endothermic reaction, while Eq. (39) is a exothermic one. As shown in Fig. 11, there must be a temperature distribution in the slag and the center of crucible is lower than that of the periphery of crucible. Since Eq. (39) is an exothermic reaction, H_2 gas evolution might occur at the center of crucible. However, the center of slag surface is pressurized by the gas from lance. Then, the position of H_2 generation (Eq. (39)) might occur at the periphery of center circle as shown in Fig. 11(a).

The solubility of hydrogen in slag is not so high, but it is the thermally activated process and temperature dependence must be high. J-Y. Park, *et al.*[29] is reported that the activation energy of hydrogen dissolution is 177 kJ, while the one in this study is 190 kJ which is in good agreement with the data of Park, *et al.* The reaction mechanism of CH_4 decomposition is evidently different between the graphite surface and the slag melt. The reaction in cooperation with slag melt must relate to the phenomena with the hydrogen dissolution into slag.

3.4. Results of CH_4 Injection into Molten Slag

As mentioned above, the injection experiments are classified into two kinds. One is the quick soaking of lance of EXP-1-1, and the other is the slow soaking of lance of EXP-1-2. The downward velocity of lance affected the amount of reaction and the solidification behavior of slag through the endothermic reaction. Finally, the path of gas raising was quite different from the lance velocity.

(1) Quick soaking of lance (EXP-1-1)

Injection experiment with quick soaking of lance was carried out. The results are shown in **Fig. 12**. When the reaction gas was introduced in the reaction tube, which is not yet injecting, hydrogen increased quickly from the decomposition reaction of CH_4. About 1 100 s, the lance was soaked quickly with the velocity of above mentioned. However, the rate of reaction did not increase, as shown in Fig. 12. The flow rate of CH_4 increased oppositely and H_2 decreased in accordance with the injection. After experiment, the solidified sample was taken out and the cross section was observed. The result is shown in **Fig. 13** in comparison with the illustration of a channel formed in the slag. In this case, since the reaction occurred rapidly in the bubbles, the solidification of slag around bubbles might occur. These solidified slag bubbles would ascending and broken at the top surface of slag and accumulated[30] (Fig. 13). The mechanism was illustrated in **Fig. 14**. In the slag, there was a channel of gas ascending and the most of slag remained in the crucible, whose sensible heat was not used for the decomposition reaction. These situations of slag, where the reaction surface was limited by the formation of channel, caused the decrease of the rate of reaction as shown in Fig. 12.

(2) Slow soaking of lance (EXP-1-2)

From the result of EXP-1-1, it was found that the formation of channel in the slag disturbed the decomposition reaction, because the reaction surface was limited by the channel formation. In this experiment, the formation of channel was inhibited by the experiment of slow soaking of lance (EXP-1-2). The results of experiment are shown in **Fig. 15**. When the injection started, a scattering of hydrogen evolution partly occurred, however, the average evolution of hydrogen did not decrease and most of CH_4 was constantly decomposed during injection.

During injection, the temperature decreased from 1 730 K to 1 650 K. From this decrease of temperature, the rate constant of ks would decrease from 7.27 to 3.38, to which the reaction rate would become a half value. If the rate of reac-

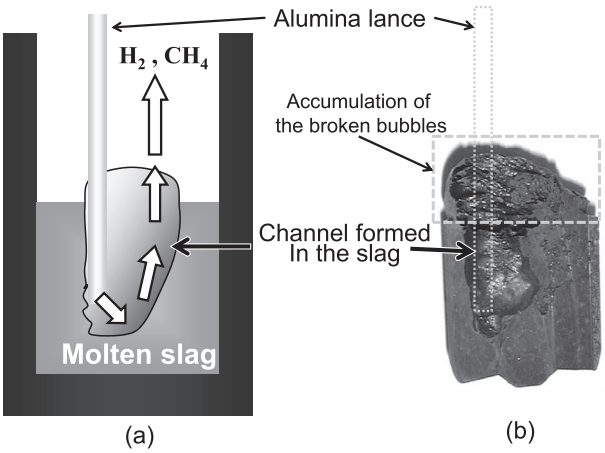

Fig. 13. (a) Illustration of bubbling experiment and (b) cross section of slag sample whit a channel of gas after experiment.

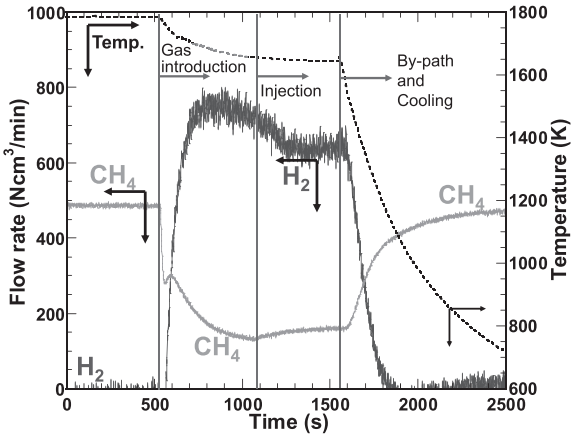

Fig. 12. Results of injection experiment with quick soaking of lance (EXP-1-1: 1 785 K, 500 Ncm^3/min CH_4).

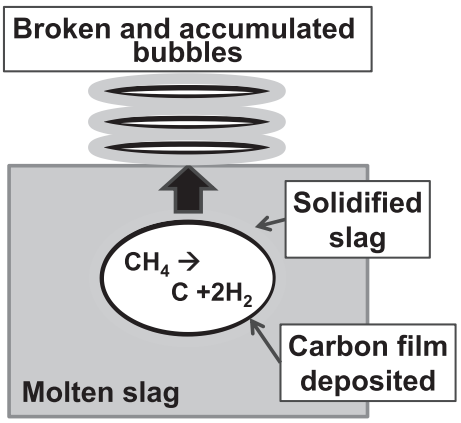

Fig. 14. Mechanism of CH_4 decomposition and slag solidification Fig. 15. Results of injection experiment with quick soaking of lance (EXP-1-2: 1 795 K, 700 Ncm^3/min CH_4).

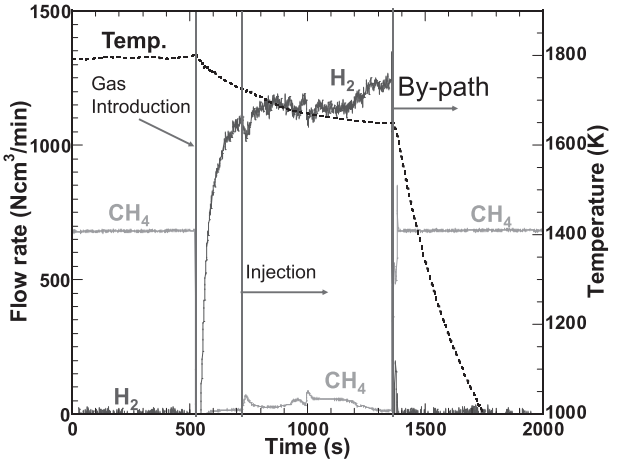

Fig. 15. Results of injection experiment with slow soaking of lance (EXP-1-2: 1 795 K, 700 Ncm^3/min CH_4).

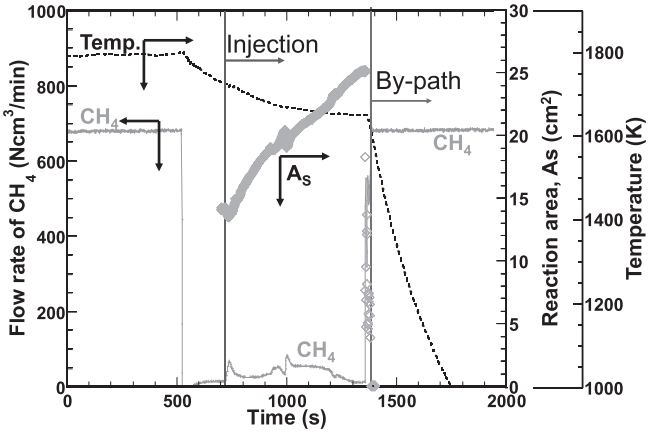

Fig. 16. Variation of estimated surface area during injection (EXP-1-2).

tion in this system was decided by only temperature, the reaction rate observed must decrease. In this study, it was considered that the apparent reaction rate during injection was resulted from the increase in total surface of reaction caused by the injection. As shown in above section, the decomposition reaction occurred in the bubble and the slag around the bubbles solidified, and then, the slag bubbles were accumulated in the top of molten slag. This phenomenon increases the reaction surface significantly. So that the area of reaction surface in the slag, 'A_S' was estimated during the injection using Eq. (40), where k'' means the apparent reaction rate during injection of CH_4 into molten slag, and A_G, k_G and k_S can use the original values obtained in the fundamental experiments (EXP-2 and EXP-3).

$$k'' = A_G k_G + A_S k_S \quad \text{.....(40)}$$

Then, the actual increase of A_S obtained are shown in **Fig. 16**.

Original surface area of slag is 8.55 cm^2 (Fig. 5). On the other hand, the surface area at the starting of injection (700 s) was about 14 cm^2. The surface area increased continuously and was about 25 cm^2 at the end of injection.

In **Fig. 17**, the injection mechanism for the slow soaking of lance and the cross section of slag sample after experiment were shown. As mentioned above, the bubble ascending to the top of surface, on which some solidified slag layer was attached, would be broken and the slag layer also broken (Fig. 14). In the case of the slow soaking of lance, the slag was foamed near the surface and soon broken (Fig. 17(a)). From this reason, the depth of bubbling will be kept constant. The broken bubbles including a carbon film and slag layer are accumulated in the top of molten slag. This mechanism might be available for making the fine slag production. Figure 17(b) shows the cross section of slag sample after experiment. Although some slag remained in the bottom of crucible, most of slag was foamed and became a powder state (some of fine slag was lost during cutting procedure of the crucible).

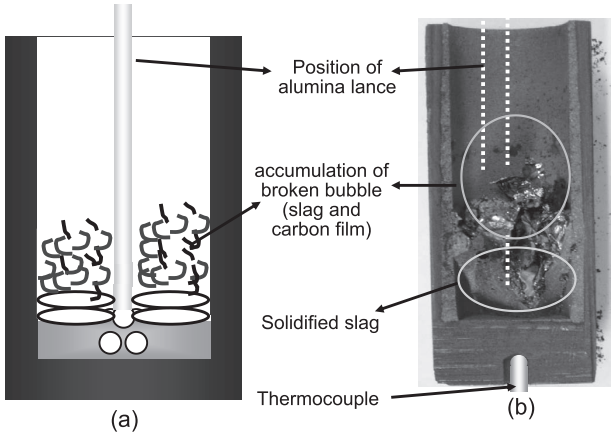

Fig. 17. (a) Illustration of slow soaking experiment of bubbling (EXP-1-2) and (b) the cross section of sample after experiment.

It is interesting to focus on the morphology of carbon formed during the injection. Two kinds of carbon were formed. The one was a film type carbon having highly crystallized one which was formed inside the bubble. The other was a soot type carbon which was observed precisely by TEM (transmission electron microscope). The details will be published in the separate paper.

4. Conclusions

The CH_4 injection experiments into molten slag were carried out and the thermal decomposition reaction CH_4 was investigated.

$$CH_4\ (g) = C + 2H_2\ (g)$$

In the fundamental experiments, kinetic analysis was performed using an empty graphite crucible and a one with slag. The rate constants for the graphite crucible, k_G and the slag, k_S, were obtained separately. Using the obtained rate constants, a kinetic analysis on the injection experiment was carried out. The results obtained are as follows:

(1) The rate constants for graphite surface and slag surface, k_G and k_S, respectively, as follows:

$$k_G\ /\ cm \cdot s^{-1} = 41.74 \times \exp\left(-\frac{51\,741}{RT}\right) \pm 0.05$$

$$k_S\ /\ cm \cdot s^{-1} = 4.053 \times 10^6 \times \exp\left(-\frac{190\,310}{RT}\right) \pm 0.05$$

(2) The CH_4 decomposition enhanced by the existence of slag melt. The mechanism of enhancement of CH_4 decomposition by slag melt was presented, in which a absorption and desorption of a radical hydrogen (H*) promoted the decomposition of CH_4.

(3) It was found that the slow soaking of the injection lance could be utilized for heat recovery of molten slag, efficiently. Moreover, the slag became a powder or flake like by the slow soaking of injection lance.

REFERENCES

1) T. Akiyama: *ISIJ Int.*, **50** (2010), 1227.
2) T. Nomura, N. Okinaka and T. Akiyama: *ISIJ Int.*, **50** (2010), 1229.
3) K. Nishioka, N. Suura, K. Ohno, T. Maeda and M. Shimizu: *ISIJ Int.*, **50** (2010), 1240.
4) Y. Kashiwaya, Y. In-Nami and T. Akiyama: *ISIJ Int.*, **50** (2010), 1245.
5) Y. Kashiwaya, Y. In-Nami and T. Akiyama: *ISIJ Int.*, **50** (2010), 1252.
6) Y. Kashiwaya, T. Akiyama and Y. In-Nami: *ISIJ Int.*, **50** (2010), 1259.
7) L. Wei and K. Ohsasa: *ISIJ Int.*, **50** (2010), 1265.
8) H. Nogami, K. Ikeuchi and K. Sato: *ISIJ Int.*, **50** (2010), 1270.
9) H. Nogami, K. Aonuma and Y. Chiba: *ISIJ Int.*, **50** (2010), 1276.
10) N. Hayashi, E. Kasai and T. Nakamura: *ISIJ Int.*, **50** (2010), 1282.
11) T. Ishihara and T. Kanno: *ISIJ Int.*, **50** (2010), 1291.
12) N. Okinaka and T. Akiyama: *ISIJ Int.*, **50** (2010), 1296.
13) N. Maruoka and T. Akiyama: *ISIJ Int.*, **50** (2010), 1305.
14) N. Maruoka, H. Purwanto and T. Akiyama: *ISIJ Int.*, **50** (2010), 1311.
15) H. Purwanto, E. Kasai and T. Akiyama: *ISIJ Int.*, **50** (2010), 1319.
16) N. Okinaka, L. Zhang and T. Akiyama: *ISIJ Int.*, **50** (2010), 1300.
17) T. Nomura, T. Oya, N. Okinaka and T. Akiyama: *ISIJ Int.*, **50** (2010), 1326.
18) HSC Chemistry for Windows Ver.5.1, Outotec Research Oy, Finland, (2002).
19) Physical and Chemical Data Book for Iron- and Steelmaking – Iron-making, ISIJ, Tokyo, (2006), 347, ISBN:4-930980-46-1 C3057.
20) Y. H. Wang, K. Tokuchi, K. Ishii, Y. Sasaki and Y. Kashiwaya: *Tetsu-to-Hagané*, **84** (1998), 55.
21) NIST kinetics Database, http://kinetics.nist.gov/kinetics/ (accessed 2011-12).
22) Y. Kashiwaya, T. Nakauchi, P. Khanh Son, S. Akiyama and K. Ishii: *ISIJ Int.*, **47** (2007), 44
23) C. P. Fenimore and G. W. Jones: *J. Phys. Chem.*, **65** (1961), 200.
24) M. J. Kurylo, G. A. Hollinden and R. B. Timmons: *Chem. Phys.*, **52** (1970), 1773.
25) J. Peeters and G. Mahnen: *Proc. Combust. Inst.*, **14** (1973), 133.
26) W. C. Gardiner, Jr., J. H. Owen, T. C. Clark, J. E. Dove, S. H. Bauer, J. A. Miller and W. J. McLean: *Proc. Combust. Inst.*, **15** (1974), 957.
27) A. Sepehrad, R. M. Marshall and H. Purnell: *J. Chem. Soc. Faraday Trans.*, **1** (1979), No. 75, 835.
28) J. W. Sutherland, M.-C. Su and J. V. Michael: *Int. J. Chem. Kinet.*, **33** (2001), 669
29) J.-Y. Park, J.-S. Han and I. Sohn: *ISIJ Int.*, **51** (2011), 1788.
30) Y. Kashiwaya and M. Watanabe: *ISIJ Int.*, **52** (2012), 1404.